Degradation Mechanism Analysis of $Ba_{0.5}Sr_{0.5}Co_{0.8}Fe_{0.2}O_{3-\delta}$ Membranes at Intermediate-Low Temperatures

Yan Liu
State Key Laboratory of Catalysis, Dalian Institute of Chemical Physics, Chinese Academy of Sciences, Dalian, 116023, China

University of Chinese Academy of Sciences, Beijing, 100039, China

Xuefeng Zhu and Weishen Yang
State Key Laboratory of Catalysis, Dalian Institute of Chemical Physics, Chinese Academy of Sciences, Dalian, 116023, China

DOI 10.1002/aic.14900
Published online June 11, 2015 in Wiley Online Library (wileyonlinelibrary.com)

The degradation of the permeation flux of $Ba_{0.5}Sr_{0.5}Co_{0.8}Fe_{0.2}O_{3-\delta}$ membranes has typically been attributed to the phase transformation of the material at intermediate temperatures. In this study, the effect of the interfacial oxygen exchange steps was considered to give an overall view of the degradation mechanism. The changes in the interfacial exchange resistances, bulk resistance, and morphologies of the membranes were investigated via physical characterizations and a permeation model. The interfacial oxygen exchange resistances increased more quickly with time than bulk resistance. Meanwhile, $BaSO_4$ particles were detected on both surfaces of the membranes, and their contents reached maximum at 650°C. However, after the membrane surfaces were coated by $Sm_{0.5}Sr_{0.5}CoO_{3-\delta}$ porous layers, the interfacial oxygen exchange resistances kept constant and the degradation rates were slowed down. The degradation was predominated by the increase of interfacial oxygen exchange resistances induced by the enrichment of $BaSO_4$ particles on membrane surfaces. *AIChE J*, 61: 3879–3888, 2015
Keywords: BSCF perovskite membrane, oxygen permeation, interfacial oxygen exchange, intermediate-low temperature, degradation mechanism

Introduction

Oxygen as an important chemical is widely used as a feed gas in many high energy consumption industrial processes in large scale,[1–8] such as coal gasification, oxy-fuel power generation, and ferrous metallurgy. The increasing demand for oxygen stems from the rapid development of oxyfuel technology for power generation and CO_2 capture.[8–15] To date, oxygen is usually separated from air via cryogenic distillation and pressure swing adsorption (PSA) methods. Although high-purity ($\geq$99.5%) oxygen is produced via cryogenic distillation, the exorbitant energy consumption, and capital costs associated with this method prevent the cheap supply of pure oxygen to the oxy-fuel process.[11,16] The cryogenic distillation technology has matured in the past century, and its efficiency can only be marginally improved in the future. In addition, although the PSA technology is simple, it can only economically supply oxygen of <95% purity at middle and small scales.[6] A novel oxygen separation technology based on mixed ionic-electronic conducting (MIEC) membranes has received considerable attention recently due to its many advantages, such as low costs, low energy consumption, simple process engineering, and flexible scales.[17–24] Ultrahigh purity oxygen can be obtained through the MIEC membrane technology due to the 100% oxygen permeation selectivity of the defect-free dense MIEC membrane.[24–26]

Perovskite (ABO_3) type MIEC membranes have been studied extensively due to their high oxygen permeability.[2,3,26,27] Among these membranes, $Ba_{0.5}Sr_{0.5}Co_{0.8}Fe_{0.2}O_{3-\delta}$ (BSCF), which was developed by our group, exhibits high oxygen permeability and has received significant attention in the last decade.[28] Its high permeability is attributed to its high ionic conductivity and catalytic activity toward both the oxygen reduction reactions (ORR) and oxygen evolution reactions (OER).[29,30] Precisely because its high catalytic activity toward ORR and OER, it has been used as cathodes in solid oxide fuel cells at intermediate-low temperatures (600–800°C) for the catalytic activation of ORR and bifunctional electrodes in rechargeable metal-air batteries for both ORR and OER.[30,31]

However, many researchers have reported that phase transformations occur on the BSCF membrane when the operation temperature is lower than 850°C. Hexagonal and plate-like phases were observed after the powder or membranes were treated in air at temperatures below 850°C for tens to hundreds hours.[32–35] The new phases have much lower ionic conductivities than the cubic phase; therefore, degradation of the oxygen permeation flux with time is frequently observed when the BSCF membranes are operated at intermediate-low

Correspondence concerning this article should be addressed to X. Zhu at zhuxf@dicp.ac.cn or W. Yang at yangws@dicp.ac.cn.

temperatures. In 2000, we reported that the oxygen permeation flux decreasing with time at 825°C and 750°C is related to the bulk phase transformation from a cubic phase to a hexagonal phase.[28] Other researchers also observed the degradation of oxygen permeation fluxes through the BSCF membrane at intermediate temperatures.[36,37] To disclose the degradation mechanism, many researchers applied characterization methods such as X-ray diffraction (XRD) and high resolution transmission electron microscopy (HRTEM) to investigate the phase structure of the fresh and the treated BSCF powders and membranes. For example, Švarcová et al. found that cubic and hexagonal (*2H* or *4H*) BSCF phases were coexisted as temperature below 850–900°C, and the amount of this hexagonal phase increased with the decrease of treating temperature.[33] Arnold et al. reported that if BSCF was annealed at temperatures below 900°C, it would decompose into a three-phase mixture of cubic perovskite $(Ba_{0.25}Sr_{0.75})(Co_{0.6}Fe_{0.4})O_{3-\delta}$, hexagonal $(Ba_{0.75}Sr_{0.25})CoO_{3-\delta}$, and monoclinic phases (space group *P2/m*).[32] It was demonstrated that BSCF would decompose into a two-phase mixture of hexagonal and cubic perovsike via a new monoclinic perovskite because +3 cobalt prefers a low-spin configuration at low temperature. Mueller et al. reported that the Ba- and Co-rich hexagonal phase (*2H*, space group $P6_3/mmc$, a = 5.63 Å, c = 4.38 Å) grew predominantly at the grain boundaries of BSCF membrane.[35] However, Efimov et al. found that aside from the hexagonal perovskite ($Ba_{0.6}Sr_{0.4}CoO_{3-\delta}$), a lamellar phase (*15R*, $Ba_{1-x}Sr_xCo_{2-y}Fe_yO_{5-\delta}$) formed in the powder and sintered ceramic after annealing at 800°C for 180–240 h in air.[38] Müller et al. also observed the lamellar substructure in the plate-like regions and revealed that these regions formed more rapidly than the bulk hexagonal phase for the BSCF sample annealed at 700°C.[34,39] In the aforementioned studies, the degradation of oxygen permeation through the BSCF membranes at intermediate temperatures was attributed to the above new phases with extremely low ionic conductivity.

For perovskite-type MIEC membranes, the oxygen permeation process usually controlled by three steps, that is, oxygen exchange on the gas-solid interface of the feed side, bulk phase diffusion of oxygen ions (the electronic conductivity is typically several orders of magnitude higher than that of the oxygen ionic conductivity), and oxygen exchange on the gas-solid interface of the permeation side.[40–42] Each step gives rise to a permeation resistance. Therefore, one question comes out, that is, is the degradation of oxygen permeation flux for BSCF membranes completely induced by the bulk phase transformation at intermediate-low temperature? To correctly answer this question, a permeation model which can distinguish the three permeation resistances should be utilized to monitor the time-dependent changes of the permeation resistances. In our previous investigation, a simple permeation model with clear physical meanings for every parameter has been established for modeling the oxygen permeation of MIEC membranes. This model has been successfully applied on perovskite and dual-phase membranes.[8,40]

In this work, we investigated the changes in the interfacial oxygen exchange resistances and the bulk diffusion resistance of BSCF at 700, 650, and 600°C using the aforementioned oxygen permeation model. With this model, the three oxygen permeation resistances across the BSCF membranes and the contribution of every resistance to the total resistance were determined; consequently, the contribution of every resistance to the degradation of the permeation flux for BSCF at intermediate-low temperatures was clearly identified.

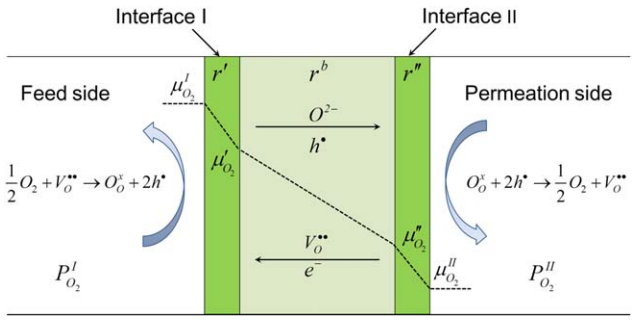

Figure 1. Schematic of the oxygen chemical potential drop across an MIEC membrane.

[Color figure can be viewed in the online issue, which is available at wileyonlinelibrary.com.]

Brief Introduction of the Model

The detailed derivation of the equations of the oxygen permeation model was presented in our previous paper.[40] This model is based on three basic assumptions. First, the properties of the oxygen ions and electrons/holes are assumed to be constant with the oxygen chemical potential, location in a given region, and over a small range of oxygen partial pressures; second, the concentration polarization resistances of oxygen diffusion from the environmental atmosphere to the gas-solid interfaces can be ignored; third, all the reaction steps (including adsorption, dissociation, charge transfer, surface diffusion, and incorporation of oxygen ions into the lattices) happen under isothermal conditions and the mass action law is valid for the oxygen exchange reactions. Figure 1 shows a schematic of the oxygen chemical potential drop across an MIEC membrane.

The total driving force for an oxygen transport process across the membrane consists of three components, namely

$$\Delta\mu^{\text{tot}}_{O_2}=\Delta\mu'_{O_2}+\Delta\mu^{b}_{O_2}+\Delta\mu''_{O_2} \tag{1}$$

where $\Delta\mu'_{O_2}$, $\Delta\mu^{b}_{O_2}$, and $\Delta\mu''_{O_2}$ are the oxygen chemical potential drop across the interface of the feed side (interface I), the membrane bulk, and the interface of the permeation side (interface II), respectively.

A general transport equation derived from Eq. 1 can then be written as follows

$$j_{O_2}=-\frac{1}{16F^2}\frac{1}{r'+r^b+r''}\Delta\mu^{\text{tot}}_{O_2}=-\frac{\Delta\mu^{\text{tot}}_{O_2}}{16F^2}\frac{1}{r^{\text{tot}}} \tag{2}$$

where $-\Delta\mu^{\text{tot}}_{O_2}/16F^2$ is the total driving force across the membrane. $r^{\text{tot}}=r'+r^b+r''$ is the total permeation resistance (area specific resistance, $\Omega\ \text{cm}^2$) and r^b, r', and r'', are the bulk diffusion resistance, and interfacial exchange resistances of the interfacial zones I and II, respectively. The total resistance can then be calculated from

$$r^{\text{tot}}=-\frac{\Delta\mu^{\text{tot}}_{O_2}}{16F^2 j_{O_2}}=-\frac{RT}{16F^2 j_{O_2}}\ln\frac{P^{\text{II}}_{O_2}}{P^{\text{I}}_{O_2}} \tag{3}$$

The permeation resistances at the interfacial regions are functions of oxygen partial pressure according to the following relationships

$$r'=r'_0\left(P^I_{O_2}/P_0\right)^{-0.5} \tag{4}$$

$$r'' = r_0'' \left(P_{O_2}^{II} / P_0 \right)^{-0.5} \quad (5)$$

where P_0, r_0', and r_0'' are the oxygen partial pressure of 1 bar and the permeation resistance across interfaces I and II, respectively, at an oxygen partial pressure of 1 bar. The influence of the oxygen partial pressure on the membrane bulk resistance can be ignored over a small range of oxygen partial pressures, without incurring significant errors. Therefore, the total permeation resistance is a function of the oxygen partial pressure of each side; that is

$$r^{\text{tot}} = r_0' \left(P_{O_2}^{I} / P_0 \right)^{-0.5} + \left(r^b + r'' \right) \quad (6)$$

$$r^{\text{tot}} = r_0'' \left(P_{O_2}^{II} / P_0 \right)^{-0.5} + \left(r^b + r' \right) \quad (7)$$

If the oxygen partial pressure on the permeation side is fixed, but varied on the feed side, one can obtain a set of data through permeation experiments to get the slope r_0' and the intercept $r^b + r''$ through linear regression of Eq. 6. Similarly, r_0'' and $r^b + r'$ can be obtained through linear regression of Eq. 7. Consequently, r_0', r_0'', and two r^b can be obtained from the linear regression of Eqs. 6 and 7. To decrease the relative deviation, average r^b values were used for modeling experiment. Then the values of r' and r'' can be calculated by introducing r_0' and r_0'' into Eqs. 4 and 5, respectively.

Experimental

Powders and membranes preparation

The BSCF powder was prepared via a combined citric acid and ethylenediamine tetraacetic (EDTA) acid method, as described in our previous papers.[28] The chemicals used in the experiments were all purchased from Sigma-Aldrich. Briefly, stoichiometric $Ba(NO_3)_2$, $Sr(NO_3)_2$, $Co(NO_3)_2 \cdot 6H_2O$ and $Fe(NO_3)_3 \cdot 9H_2O$ were dissolved in deionized water, and then citric acid and EDTA acid were subsequently added to the aqueous solution of the nitrates. The molar ratio of the total metal ions:citric acid:EDTA acid was 1:1.5:1. $NH_3 \cdot H_2O$ was used to adjust the pH value of the solution to 6–8. The solution was then heated under constant stirring on a hot plate to obtain a dark purple gel. This gel was subsequently heated to selfignition to form an ash. Pure cubic perovskite phase was obtained by calcining the resultant ash in air at 950°C for 5 h. The BSCF powders were pressed into green disks at ~200 MPa in an 18 mm diameter stainless steel die. Dense disk-type membranes were then obtained by sintering the green disks at 1150°C for 3 h. After the membranes were polished to 0.5 mm in thickness by using 500-mesh waterproof sandpaper, they were ultrasonically cleaned in ethanol before the permeation experiments. $Sm_{0.5}Sr_{0.5}CoO_{3-\delta}$ (SSC) powder was also synthesized via the combined citric acid and EDTA acid method. The slurry used for coating BSCF membrane surfaces was made of terpineol and SSC powder in a weight ratio of 1:1. Porous SSC layers with thickness of 10–20 μm were formed on BSCF membrane surfaces after calcining at 960°C for several hours.

The sulfur content in the BSCF powder was determined as following. First, α-Al_2O_3 powder with particle size of ~10 μm was treated by HCl, washed with deionized water, centrifuged and dried in an oven at 120°C to remove potential impurities. Second, BSCF (2.00 g) powder was dissolved in excess HCl, then 20 mg of the treated α-Al_2O_3 was added into the solution. The function of α-Al_2O_3 powder is to dilute $BaSO_4$ particles because $BaSO_4$ is too little to be facilely weighted. 0.024 g precipitant was obtained after washing and drying. The weight ratio of sulfur in the precipitant was determined by energy dispersive X-ray spectroscopy (EDS) analysis, and gave an average value of 2.0%. Thus the sulfur content was 240 ppm in BSCF powder.

Measurements of oxygen permeation

The membranes were sealed with silver rings at 961°C (the melting point of silver). The effective membrane areas were around 1.0 cm^2 after sealing. The operation temperature was controlled by a microprocessor temperature controller (Model AI-708, Xiamen Yuguang Electronics Technology Research Institute, China) within ±1°C with a K-type thermocouple. Dry synthesized air (O_2: 21 vol %, 150 mL min^{-1}) and high purity helium (50 mL min^{-1}) were used as the feed and sweep gases, respectively. The flow rates of these gases were controlled by mass flow controllers (Models D07-7A/ZM, Beijing Jianzhong Machine Factory, China). All the gases were passed through cylinders (Ø 50 mm × 300 mm) filled with 50 vol % KOH pellets and 50 vol % 4A zeolite granules before they were introduced into the permeation reactor. Effluents were analyzed by a gas chromatography (Agilent 6890) equipped with a thermal conductivity detector and a 3 m 5 A zeolite column. Oxygen permeation fluxes through the BSCF membranes were calculated based on the flow rates of the effluents and the oxygen concentration in the effluents. The leakages due to the imperfect sealing were no more than 2% for all the oxygen permeation experiments, and subtracted when calculating the permeation fluxes.

Characterizations

The crystal structure of the BSCF powders and membranes were determined by XRD (Rigaku D/Max-RB, Cu Kα radiation) in a 2θ range of 20–80° with a scanning rate of 5° min^{-1}. Surface morphologies of the membranes were observed on a Field-Emission Scanning Electron Microscope (Quanta 200 FEG, FEI Company) operated at 20 kV. The elemental composition information of the spent membrane surfaces were determined by the EDS operated at a lower voltage of 10 kV.

Results and Discussion

Permeation model analysis of the BSCF membranes

Figure 2 shows the time-dependent oxygen permeation fluxes of the BSCF membranes at 700, 650, and 600°C. The oxygen permeation fluxes all decreased with time during the 100 h on-stream. Previous studies suggested that the degradation of the oxygen permeation flux results from the phase transformation of the BSCF membrane at temperature below 850°C, and the degradation rate increases with the decrease of operation temperature in the range of 700–850°C.[28,36,37] However, as shown in the figure, the oxygen permeation flux decreased fastest at 650°C among the three investigated temperatures. For MIEC membranes, the oxygen permeation process is controlled by three steps, that is, interfacial oxygen exchange at feed side, bulk phase diffusion, and interfacial oxygen exchange at permeation side. The three steps correspond to three permeation resistances, and an increase of any permeation resistance can lead to the degradation of oxygen permeation flux.

To disclose the degradation mechanism of BSCF at intermediate-low temperatures, an oxygen permeation model was used to monitor the changes in the interfacial exchange

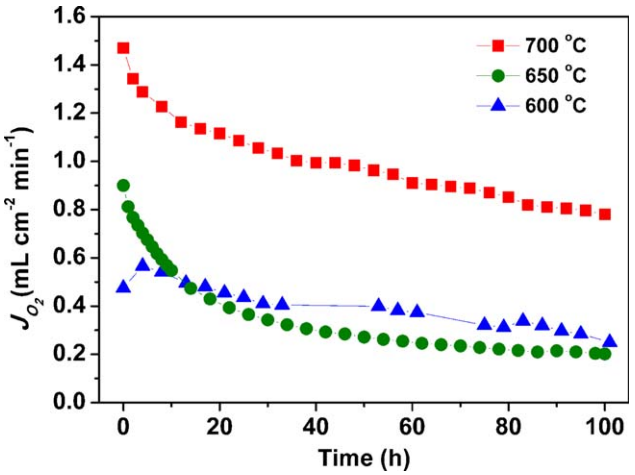

Figure 2. Time-dependent oxygen permeation fluxes of the BSCF membranes at 700, 650, and 600°C.

The flow rates of the feed (air) and sweep (He) gases are 150 and 50 mL cm^{-2} min^{-1}, respectively. [Color figure can be viewed in the online issue, which is available at wileyonlinelibrary.com.]

and bulk diffusion resistances during a 100 h on-stream at 700, 650, and 600°C. At each operation temperature and oxygen partial pressure gradient, a total permeation resistance r^{tot} can be calculated using Eq. 3. When the oxygen partial pressure is fixed at the permeation side and simultaneously varied at the feed side, then r'_0 (the slope) and r^b+r'' (the intercept) can be acquired by means of linear regression of Eq. 6. Similarly, when the oxygen partial pressure of the feed side is fixed and that of permeation side is simultaneously varied, r''_0 and r^b+r' can be obtained by the linear regression of Eq. 7. Then the values of r' and r'' can be calculated by introducing r'_0 and r''_0 into Eq. 4 and Eq. 5, respectively. After that, two r^b values will be obtained from Eqs. 6 and 7, respectively. In principle, the two r^b values should be the same; however, they are different due to the inevitable experimental errors. In this article, average values of r^b were used. In a typical experiment, six to eight sets of data should be collected at least to minimize the regression errors. Usually, it took about 2∼3 h to collect these data. However, the oxygen permeation fluxes of the BSCF membranes decreased rapidly with time at intermediate-low temperatures, as a result additional errors were introduced to the r'_0 and r''_0. In fact, the regressed r'_0 and r''_0 were the average values in the data collecting periods (2∼3 h). Therefore, the regressed r'_0 and r''_0 were still effective to reflect the time-dependent changes in the interfacial exchange resistances. However, the additional errors have great influences on values of the bulk diffusion resistances because they are much smaller than the interfacial exchange resistances, which will be shown in the following sections. Therefore, except r^b, the variations of r' and r'' with time are plotted in Figure 3.

At 700°C, the interfacial exchange resistance at the permeation side r'' increased with time and was always larger than that at the feed side r' which almost kept constant during the ∼100 h testing. After the ∼100 h testing, the r'/r'' ratio decreased from 0.80 ($t = 10$ h) to 0.58 ($t = 100$ h). As the temperature was decreased to 650°C, both r' and r'' increased with time, while r' increased faster than r'', and after ∼100 h testing, the r'/r'' ratio increased from 1.8 ($t = 10$ h) to 3.1 ($t = 100$ h). A similar trend was observed on the testing at 600°C; that is, both r' and r'' increased with time and the r'/r'' ratio increased from 2.1 ($t = 10$ h) to 2.8 ($t = 100$ h) after ∼100 h. In general, r' and r'' should increase regularly with the decrease of the operation temperature, because a higher temperature is beneficial to the interfacial oxygen exchange

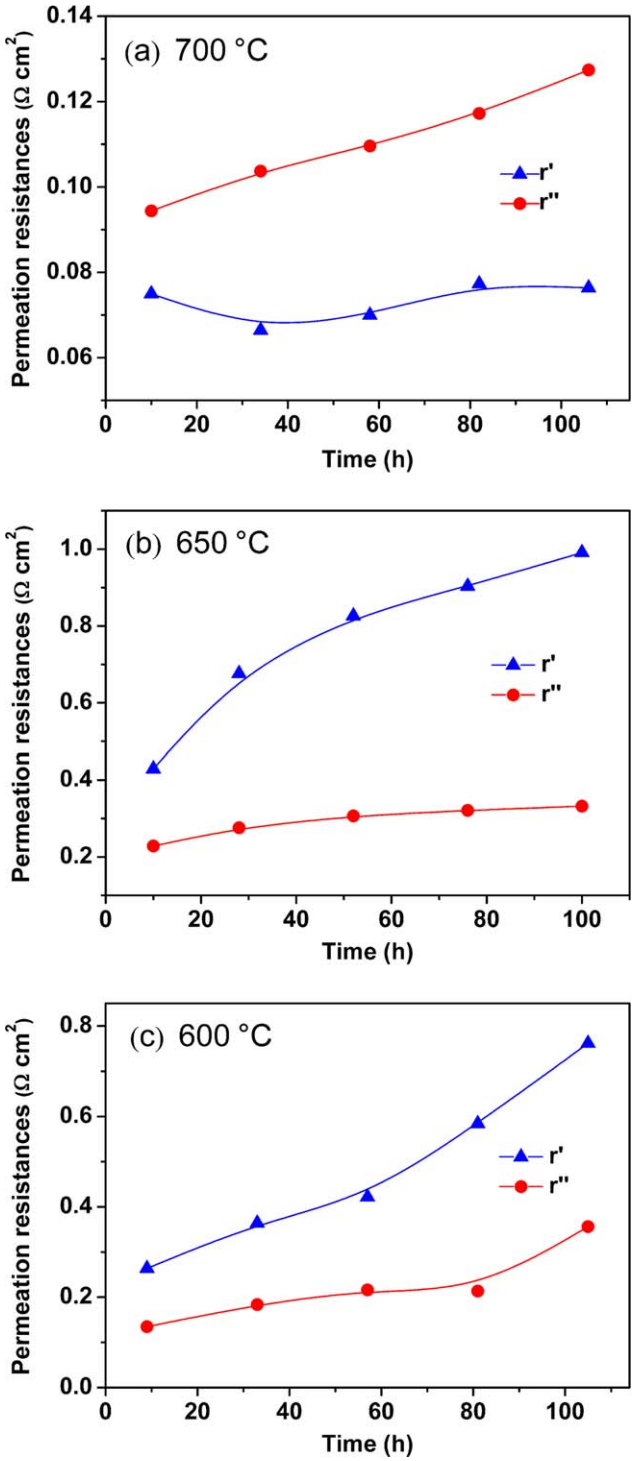

Figure 3. Time-dependent changes in the permeation resistances of the interfaces at the feed side (r') and permeation side (r''), respectively, of the BSCF membranes.

(a) 700°C, (b) 650°C, and (c) 600°C. The oxygen partial pressure of the feed and permeation sides are 0.21 bar and 0.01 bar, respectively. [Color figure can be viewed in the online issue, which is available at wileyonlinelibrary.com.]

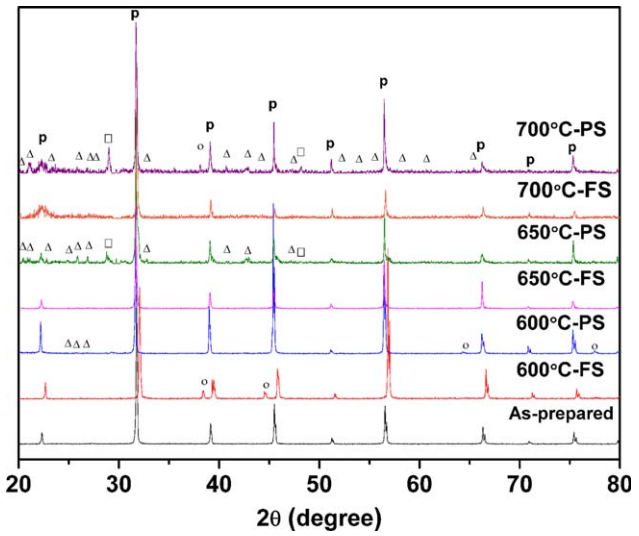

Figure 4. XRD diffraction patterns of the BSCF powder and spent BSCF membranes at 700, 650 and 600°C.

PS: permeation side, FS: feed side. The "p", triangle, circle, and rectangle denote the diffraction peaks of cubic perovskite, $BaSO_4$, silver, and BaO, respectively. [Color figure can be viewed in the online issue, which is available at wileyonlinelibrary.com.]

reactions. However, the maximum values of r' and r'' were observed at 650°C instead of 600°C. This unusual result indicates that some changes occurred on the membrane surfaces, which resulted in an abnormal increase of r' and the fastest degradation of oxygen permeation flux at 650°C. Although the bulk diffusion resistance could not be reliably acquired by the model investigation, the increase in the total interfacial exchange resistances ($r' + r''$) at all temperatures indicates that degradation of the oxygen permeation flux is related to the interfacial exchange reactions.

Characterizations of BSCF membranes

To understand the changes of the interfacial exchange resistances at different operation temperatures, the spent membranes were characterized by XRD and SEM/EDS. Figure 4 shows the XRD patterns of the as-prepared BSCF powder and both surfaces of the spent BSCF membranes operated at different temperatures. As shown in Figure 4, besides the perovskite diffraction peaks, $BaSO_4$ diffraction peaks were observed on the both surfaces of the spent membranes. The intensity of the $BaSO_4$ peaks on the permeation sides was stronger than those on the feed sides. This observation concurs with our previous finding that the migration of sulfur (~20 ppm in $BaCe_{0.1}Co_{0.4}Fe_{0.5}O_{3-\delta}$ membranes) from the membrane bulk to the surface to form $BaSO_4$ is related to the oxygen chemical potential gradient, and results in that the content of the sulfates at permeation sides are higher than those on feed sides. It is precisely because the sulfur impurities lead to the degradation of oxygen permeation fluxes for those membranes with stable structures at low temperature.[43] In this study, the sulfur content is about 240 ppm in BSCF. The results of thermodynamic calculation show that $BaSO_4$ is preferential to form at intermediate-low temperatures than the Sr counterpart. Therefore, only $BaSO_4$ particles were observed on the membrane surfaces.

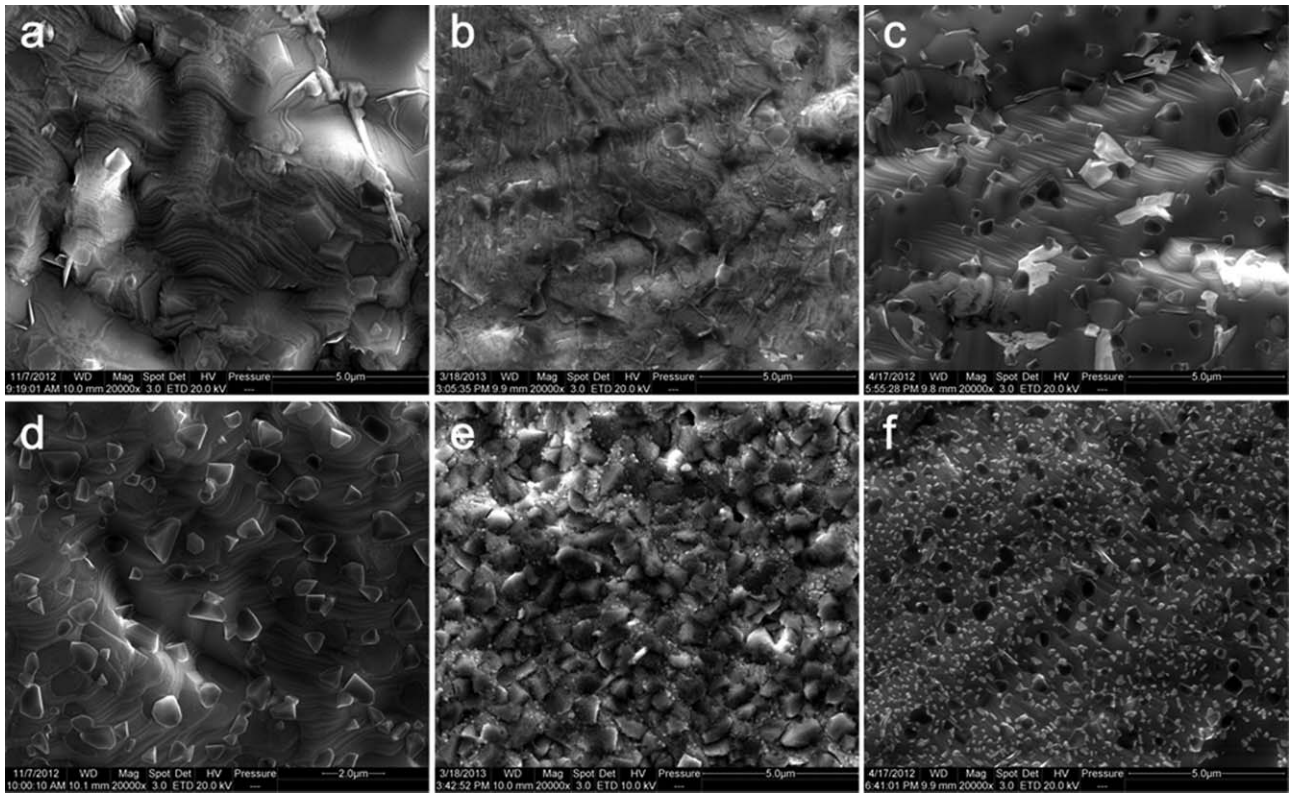

Figure 5. SEM images of the BSCF membrane surfaces after 100 h on-stream at 700°C (a, d), 650°C (b, e), 600°C (c, f), respectively.

(a, b, and c) are the images of the feed side surfaces, respectively; (d, e, and f) are the images of the permeation side surfaces, respectively.

Table 1. The Sulfur Contents of the Membrane Surfaces after ~100 h On-Stream at Different Temperatures

Temperature (°C)	S Content (at %, feed side)	S Content (at %, permeation side)
700	0.6	1.9
650	1.0	9.3
600	0.7	1.7

The intensities of the $BaSO_4$ peaks of both sides increased in the order of 600, 700, 650°C. In addition, the peaks corresponding to silver, in the diffraction patterns of the feed side of the membrane tested at 600°C, and the permeation side of the membranes tested at 700 and 600°C, resulted from the silver ring that was used as the sealant. The BaO phase was also detected on the permeation sides of the spent membranes, and its diffraction intensity decreased in the order of 700, 650, 600°C. However, peaks associated with the hexagonal phase were absent from the XRD patterns. This absence may be attributed to the fact that a smaller amount of hexagonal phase formed at the lower operation temperatures (600–700°C) in this study compared with those reported at higher temperatures (700–850°C) in other studies.[38,39]

SEM and EDS were used to determine the morphological and compositional changes on the surfaces of the spent BSCF membranes after ~100 h on-stream. As shown in Figure 5 a–f, $BaSO_4$ grains (protuberant grains on membrane surface) were observed on the both sides of the three spent membranes. There were more $BaSO_4$ particles on the permeation sides than on the feed sides; this result concurs with the XRD analysis. The corresponding sulfur contents, determined by EDS analysis, are listed in Table 1. The BSCF membrane operated at 650°C had significantly higher sulfur contents than the membranes operated at 600 and 700°C. The high sulfur contents on the membrane surfaces increased the interfacial oxygen exchange resistances, as revealed by the higher r' and r'' at 650°C, relative to those at 600 and 700°C, as shown in Figure 3. That may explain the fastest degradation rate of the oxygen permeation flux occurring at 650°C, instead of at 600°C. At elevated temperatures, $BaSO_4$ decomposed gradually into BaO, SO_2, and O_2, so the diffraction peaks of BaO could be identified on the permeation sides of the spent BSCF membranes operated at 650 and 700°C. In a flowing atmosphere, SO_2 and O_2 can be taken away from the permeator, thereby breaking the balance of the decomposition reaction. A schematic of the temperature-dependent rates of $BaSO_4$ decomposition and sulfur migration are plotted in Figure 6. At 700°C, sulfur is readily migrated from the bulk of the membrane to the surfaces and subsequent formation of $BaSO_4$ is correspondingly fast; meanwhile, the decomposition rate of $BaSO_4$ is fast, as shown in zone III in Figure 6. As a result, fewer sulfur elements were detected on the membrane surfaces. Compared with those at 700°C, the migration and decomposition rates are both slower (zone I) at 600°C; consequently, only a few sulfur elements were detected on the membrane surfaces. However, when the membrane was operated at 650°C, the migration rate is significantly higher than the decomposition rate (zone II), which leads to a rapid enrichment of sulfur elements on the membrane surfaces. That is why the sulfur contents on the surfaces of the membrane operated at 650°C were higher than

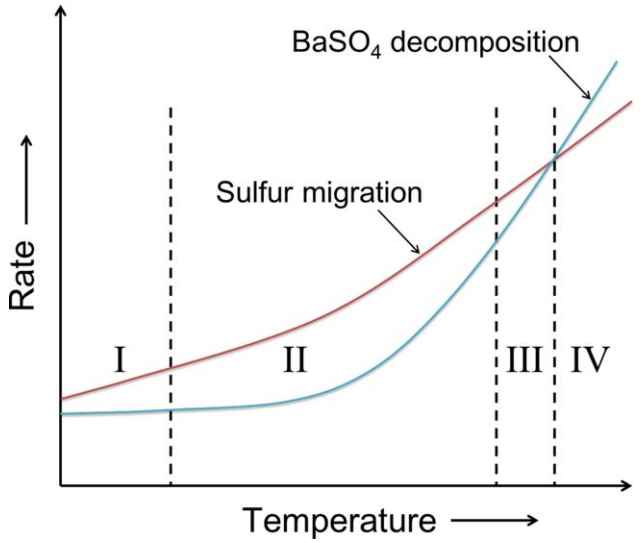

Figure 6. Schematic of the temperature-dependent rates of $BaSO_4$ decomposition and sulfur migration.

[Color figure can be viewed in the online issue, which is available at wileyonlinelibrary.com.]

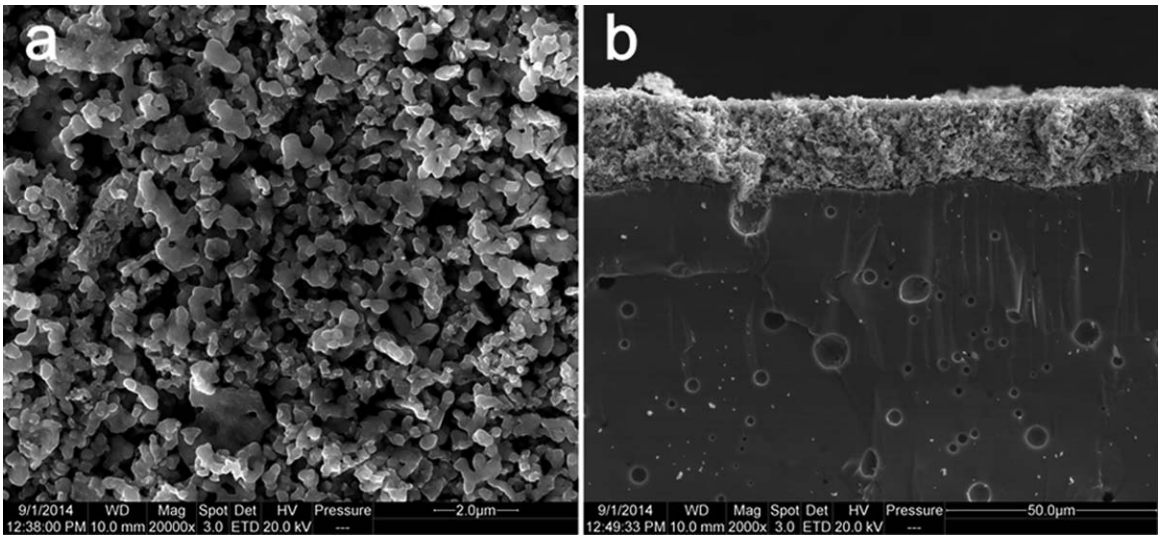

Figure 7. SEM images of the BSCF/SSC membrane. (a) Top and (b) cross-sectional views of the SSC porous layer.

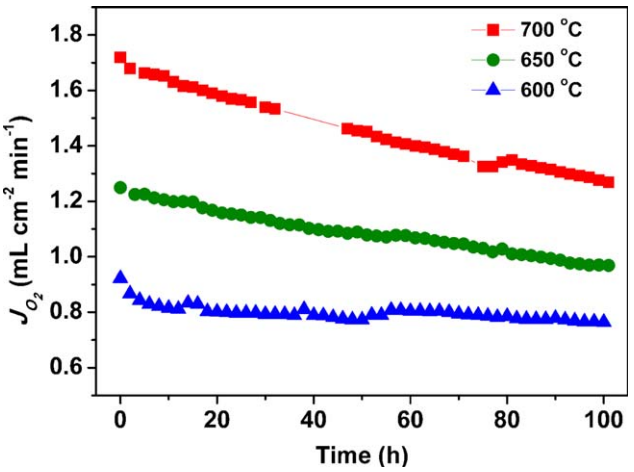

Figure 8. Time-dependence of oxygen permeation fluxes of the BSCF/SSC membranes at 700, 650, and 600°C.

The flow rates of the feed (air) and sweep (He) gases are 150 and 50 mL cm^{-2} min^{-1}, respectively. [Color figure can be viewed in the online issue, which is available at wileyonlinelibrary.com.]

those at 700 and 600°C. At sufficiently high temperatures, if the $BaSO_4$ decomposition rate exceeds the rate of sulfur migration from the bulk to the surface (zone IV), $BaSO_4$ grains will not be observed on membrane surfaces. The aforementioned results suggest that $BaSO_4$ has a greater influence on the interfacial oxygen exchange of the feed side than that of the permeation side. However, the details of the mechanism, which leads to this greater influence, remain unclear.

Permeation model analysis of the BSCF/SSC membranes

$BaSO_4$ is chemically inert toward oxygen activation and transport, and as such, leads to an increase in the interfacial oxygen exchange resistances; these resistances, in turn, results in degradation of the permeation performance of MIEC membranes. In our previous work, we found that coating $Sm_{0.5}Sr_{0.5}CoO_{3-\delta}$ (SSC) porous layers on both surfaces of MIEC membranes can result in the migration of the $BaSO_4$ grains from the membrane surfaces to the porous SSC layers.[43] The degradation of the oxygen permeation flux, which is induced by the sulfur enrichment on the membrane surfaces, can therefore, be prevented. As such, the BSCF membranes coated with SSC porous layers on both surfaces (BSCF/SSC) were used in the current oxygen permeation experiments. Figure 7 shows the top and cross-sectional views of the typical morphologies of the SSC porous layers. The thickness of the SSC porous layers was $\sim$ 20 μm and the SSC particles had a size of 0.5$\sim$1 μm. The time-dependent oxygen permeation fluxes at 700, 650, and 600°C are shown in Figure 8. As the figure shows, the oxygen permeation fluxes of the SSC-coated membranes were all higher than those of the noncoated membranes. The SSC porous layers have two functions, one is to

Table 2. The Degradation Rates per 100 h of Oxygen Permeation Flux of BSCF and BSCF/SSC Membranes at Different Temperatures

	Degradation Rates per 100 h of Oxygen Permeation Flux	
Temperature (°C)	BSCF	BSCF/SSC
700	47%	26%
650	78%	22%
600	47%	17%

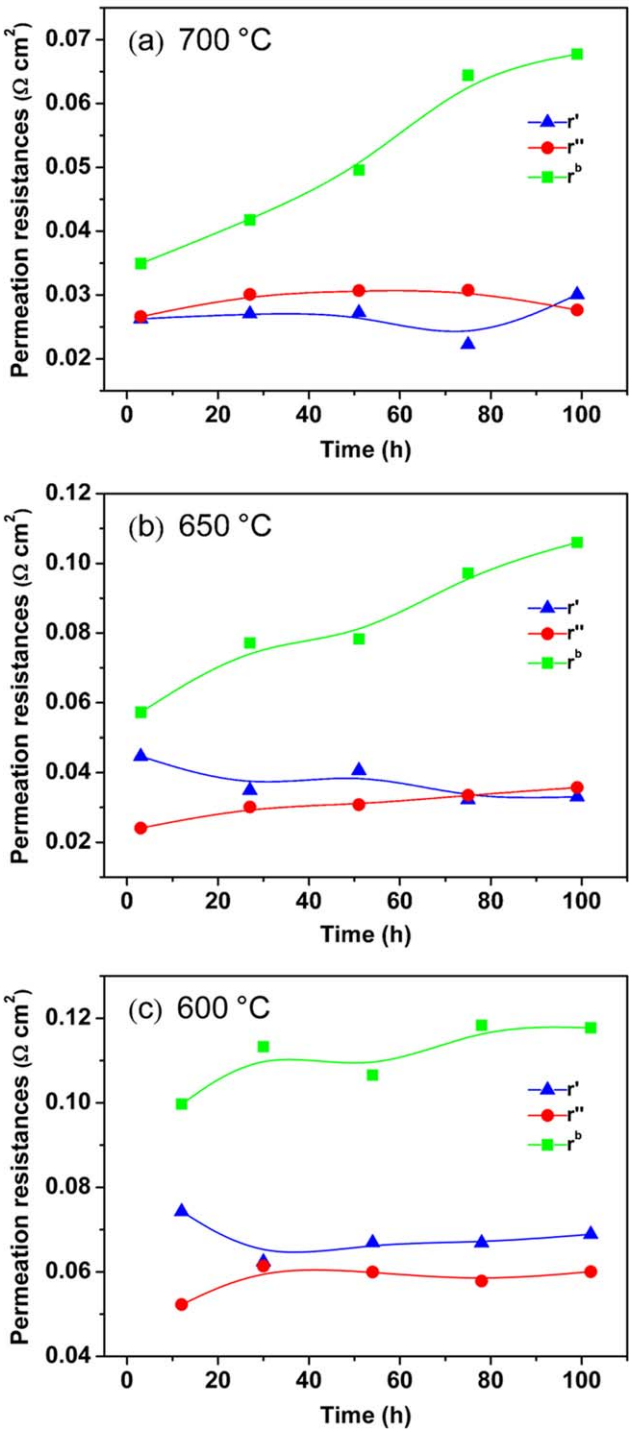

Figure 9. Time-dependence of the interfacial exchange resistances on the feed side (r') and permeation side (r''), and the bulk diffusion resistance (r^b) of the BSCF/SSC membranes.

(a) 700°C, (b) 650°C, and (c) 600°C. The oxygen partial pressure of the feed and permeation sides are 0.21 bar and 0.01 bar, respectively. [Color figure can be viewed in the online issue, which is available at wileyonlinelibrary.com.]

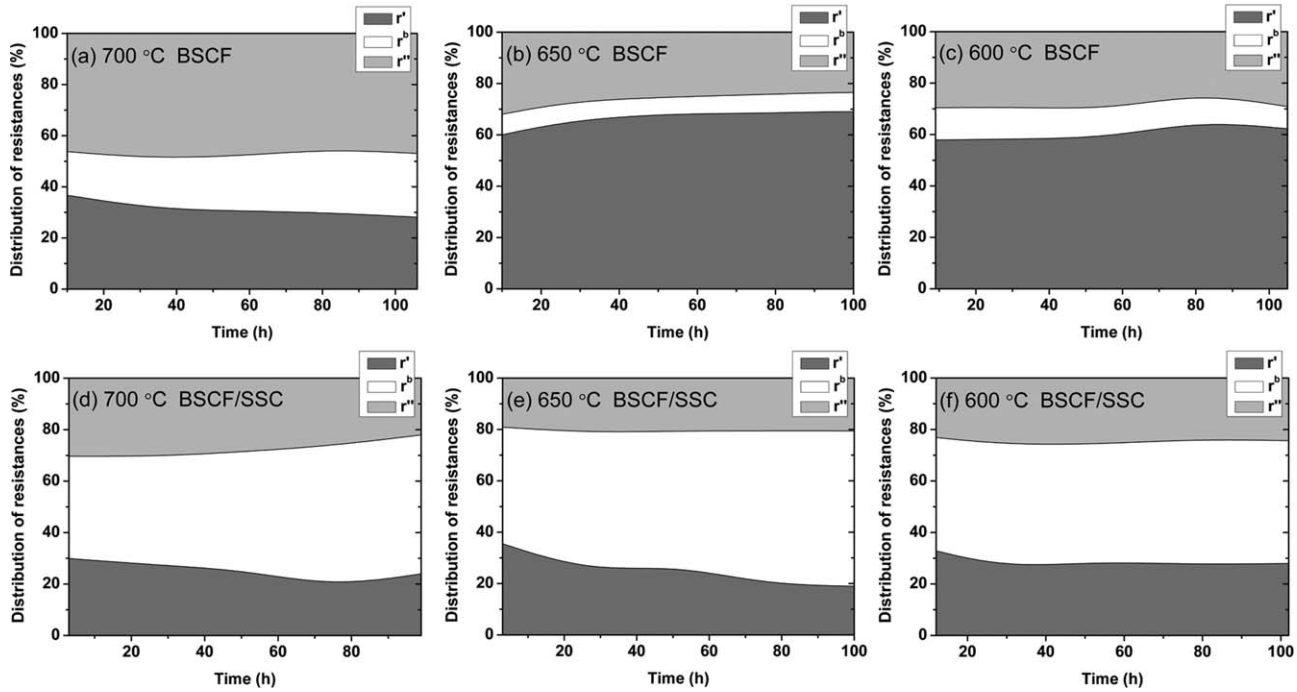

Figure 10. Time-dependence of the permeation resistance distributions of the BSCF (a, b, and c) and the BSCF/SSC (d, e, and f) membranes at 700, 650, and 600°C.

The oxygen partial pressure of the feed and permeation sides are 0.21 bar and 0.01 bar, respectively.

catalyze the interfacial oxygen exchange reactions due to its high oxygen catalytic activity and another is to accommodate sulfur impurities owing to its high surface area, and thereby eliminate the negative effects of sulfur impurities on the interfacial oxygen exchange reactions. Thus, the total interfacial oxygen exchange resistances were significantly lower after the membranes coated by SSC porous layers than those of non-coated counterparts. Table 2 compares the degradation rates of the BSCF and BSCF/SSC membranes and reveals that the oxygen permeation fluxes of the latter degrade more slowly than those of the former. For example, at 650°C, the oxygen permeation flux of the coated and uncoated membranes degraded by 22% and 78%, respectively, during 100 h on-streams.

To identify the degradation mechanism of the BSCF/SSC membranes, the oxygen permeation model was used to monitor the changes in the three permeation resistances at 700, 650, and 600°C. The results of the permeation model analysis are shown in Figure 9. Unlike that happened on the BSCF membrane, as the membranes coated by SSC (i.e., BSCF/SSC) the permeation fluxes degraded slowly, that allowed us to acquire r^b values with relatively small errors. In addition, the interfacial oxygen exchange resistances of the feed side (interface I) r', and the permeation side (interface II) r'', exhibited only limited fluctuation during the ~100 h on-stream at each temperature; this indicates that the SSC porous layers are effective to eliminate the negative influence of sulfur impurities. However, the bulk diffusion resistances (r^b) increased gradually with time at every operation temperature. Therefore, it reveals that some new phases produced in the membrane bulk during the on-stream, which block oxygen ions transport across the membrane at intermediate-low temperatures. This phenomenon has been extensively investigated by many researchers using XRD, SEM/EDX, and HRTEM/SEAD characterizations.[32–35,38,39] After ~100 h on-stream, r^b increased by 94%, 83%, and 18% for the membranes operated at the temperatures of 700, 650, and 600°C, respectively, which reveals that the phase transformation proceeded faster at higher temperatures than at lower ones. Combined with other researchers' findings on the phase transformation rate and the above result, we can conclude that the plot of the phase transformation rate against temperature is a volcano-type curve, and the maximum should appear at a temperature around 700°C.

Distributions of permeation resistances for BSCF and BSCF-SSC membranes

The analysis, so far, clearly shows that the degradation of the oxygen permeation flux of BSCF membranes at intermediate-low temperatures was influenced by two factors, that is, (1) the phase transformation, and (2) the increase in the interfacial oxygen exchange resistances induced by sulfur enrichment under the oxygen chemical potential gradient. The time-dependent permeation resistance distribution can reveal the dominant contributing factor to this degradation. Figure 10 shows the distributions of the permeation resistances of the BSCF and BSCF/SSC membranes at different temperatures. To draw these pictures, we assumed that the BSCF and BSCF/SSC membranes had the same bulk resistances. In the case of the BSCF membranes, the interfacial oxygen exchange resistances ($r'+r''$) contributed a substantially larger fraction of the total resistance than the bulk diffusion resistance at each temperature (Figures 10a–c); therefore, the interfacial exchange kinetics was the rate limiting steps in the investigated temperature range. Especially, the bulk diffusion resistance was only ~10% at 650°C. As a result, changes in the interfacial exchange kinetics had a significant influence on the permeation flux. However, for the BSCF/SSC membranes, the total interfacial oxygen exchange resistances were only slightly higher than the bulk diffusion resistances at the initial stage of

permeation experiments at 700 and 650°C (Figures 10 d,e), but this trend gradually reversed with time due to the gradually increase in the bulk diffusion resistances. In the case of the BSCF/SSC membrane operated at 600°C, the total interfacial exchange resistances and the bulk diffusion resistance were almost equal for the entire permeation experiment (Figure 10f); that is, the oxygen permeation process was jointly controlled by the interfacial oxygen exchange and the bulk diffusion under an oxygen partial pressure gradient of 0.21 bar/0.01 bar at 600°C. Basing on the results shown in Figure 10, we conclude that the degradation of the interfacial oxygen exchange kinetics, induced by sulfur enrichment, is the dominant factor that leads to the degradation of the oxygen permeation flux at intermediate-low temperatures; bulk phase transformation is only a minor contributor to the degradation.

Conclusions

Oxygen permeation fluxes of BSCF and BSCF/SSC membranes decreased with time at intermediate-low temperatures. The degradation mechanism of BSCF membranes was investigated by an oxygen permeation model. The r' and r'' of the BSCF membranes both increased with time. The $BaSO_4$ crystal phase, which is inert toward oxygen activation, was detected on both sides of the BSCF membranes. In contrast, r' and r'' of the BSCF/SSC membranes were almost constant. This indicates that the SSC porous layer has the ability to eliminate the negative effect of $BaSO_4$ by moving $BaSO_4$ from the membrane surface to the SSC porous layers under an oxygen chemical potential gradient. Furthermore, the increase in r^b of the BSCF/SSC membranes with time confirms the occurrence of a bulk phase transformation at intermediate-low temperatures. The resistance distribution reveals that the interfacial exchange kinetics is the rate limiting step for the BSCF membranes at intermediate-low temperatures; therefore, changes in the kinetics have a significant influence on the oxygen permeation flux. However, in the case of the BSCF/SSC membranes, the permeation rate limiting step gradually shifts with time from interfacial exchanges to bulk diffusion at 700 and 650°C, while it becomes jointly controlled by interfacial exchanges and bulk diffusion as the operation temperature decreased to 600°C. Moreover, sulfur enrichment is the dominant contributing factor to the degradation of the oxygen permeation flux, which leads to the deceleration of interfacial oxygen exchange kinetics at intermediate-low temperatures; however, the bulk phase transformation, which increases the bulk diffusion resistance, is a minor contributor to the degradation of the BSCF membrane at intermediate-low temperatures.

Acknowledgments

The authors gratefully acknowledge the financial support of National Natural Science Foundation of China (21271169 and 21476225) and the Key Research Program of the Chinese Academy of Sciences.

Notation

F = Faraday constant
j_{O_2} = oxygen permeation flux
P_{O_2} = oxygen partial pressure
P_0 = oxygen partial pressure of 1 bar
r = area specific resistance of species i
r_0 = area specific resistance at oxygen partial pressure of 1 bar
R = gas constant
T = temperature
$\Delta\mu_i$ = chemical potential difference of species i across the membrane
b = membrane bulk
I = gas phase of feed side
II = gas phase of permeation side
tot = including both interfaces and membrane bulk
$'$ = interface I
$''$ = interface II

Literature Cited

1. Bouwmeester HJM. Dense ceramic membranes for methane conversion. *Catal Today*. 2003;82:141–150.
2. Zhang K, Sunarso J, Shao Z, Zhou W, Sun C, Wang S, Liu S. Research progress and materials selection guidelines on mixed conducting perovskite-type ceramic membranes for oxygen production. *RSC Adv*. 2011;1:1661–1676.
3. Hashim SM, Mohamed AR, Bhatia S. Current status of ceramic-based membranes for oxygen separation from air. *Adv Colloid Interface Sci*. 2010;160:88–100.
4. Yang W, Wang H, Zhu X, Lin L. Development and application of oxygen permeable membrane in selective oxidation of light alkanes. *Top Catal*. 2005;35:155–167.
5. Zhu X, Li Q, Cong Y, Yang W. Syngas generation in a membrane reactor with a highly stable ceramic composite membrane. *Catal Commun*. 2008;10:309–312.
6. Belaissaoui B, Moullec YL, Hagi H, Favre E. Energy efficiency of oxygen enriched air production technologies: cryogeny vs membranes. *Sep Purif Technol*. 2014;125:142–150.
7. Li H, Liu Y, Zhu X, Cong Y, Xu S, Xu W, Yang W. Oxygen permeation through Ca-contained dual-phase embranes for oxyfuel CO_2 capture. *Sep Purif Technol*. 2013;114:31–37.
8. Zhu X, Liu H, Cong Y, Yang W. Novel dual-phase membranes for CO_2 capture via an oxyfuel route. *Chem Commun*. 2012;48:251–253.
9. Norton TT, Ortiz-Landeros J, Lin Y S. Stability of La-Sr-Co-Fe oxide-carbonate dual-phase membranes for carbon dioxide separation at high temperatures. *Ind Eng Chem Res*. 2014;53:2432–2440.
10. Schulz M, Kriegel R, Kämpfer A. Assessment of CO_2 stability and oxygen flux of oxygen permeable membranes. *J Membr Sci*. 2011; 378:10–17.
11. Habib MA, Badr HM, Ahmed SF, Ben-Mansour R, Mezghani K, Imashuku S, la O' GJ, Shao-Horn Y, Mancini ND, Mitsos A, Kirchen P, Ghoneim AF. A review of recent developments in carbon capture utilizing oxy-fuel combustion in conventional and ion transport membrane systems. *Int J Energy Res* 2011;35:741–764.
12. Smart S, Lin CXC, Ding L, Thambimuthu K, Diniz da Costa JC. Ceramic membranes for gas processing in coal gasification. *Energy Environ Sci*. 2010;3:268–278.
13. Engels S, Beggel F, Modigell M, Stadler H. Simulation of a membrane unit for oxyfuel power plants under consideration of realistic BSCF membrane properties. *J Membr Sci*. 2010;359:93–101.
14. Luo H, Efimov K, Jiang H, Feldhoff A, Wang H, Caro J. CO_2-stable and cobalt-free dual-phase membrane for oxygen separation. *Angew Chem Int Edit*. 2011;50:759–763.
15. Wei Y, Wang Y, Tang J, Li Z, Wang H. Oxy-fuel combustion for CO_2 capture using a CO_2-tolerant oxygen transporting membrane. *AIChE J*. 2013;59:3856–3862.
16. He Y, Zhu X, Li Q, Yang W. Perovskite oxide absorbents for oxygen separation. *AIChE J*. 2009;55:3125–3133.
17. Tan X, Wang Z, Liu H, Liu S. Enhancement of oxygen permeation through $La_{0.6}Sr_{0.4}Co_{0.2}Fe_{0.8}O_{3-\delta}$ hollow fibre membranes by surface modifications. *J Membr Sci*. 2008;324:128–135.
18. Tan X, Liu Y, Li K. Preparation of LSCF ceramic hollow-fiber membranes for oxygen production by a phase-inversion/sintering technique. *Ind. Eng. Chem. Res*. 2005;44:61–66.
19. Watenabe K, Yuasa M, Kida T, Teraoka Y, Yamazoe N, Shimanoe K. High-performance oxygen-permeable membranes with an asymmetric structure using $Ba_{0.95}La_{0.05}FeO_{3-\delta}$ perovskite-type oxide. *Adv Mater*. 2010;22:2367–2370.
20. Asadi AA, Behrouzifar A, Iravaninia M, Mohammadi T, Pak A. Preparation and oxygen permeation of $La_{0.6}Sr_{0.4}Co_{0.2}Fe_{0.8}O_{3-\delta}$ (LSCF) perovskite-type membranes: experimental study and mathematical modeling. *Ind Eng Chem Res*. 2012;51:3069–3080.
21. Cheng Y, Zhao H, Teng D, Li F, Lu X, Ding W. Investigation of Ba fully occupied A-site $BaCo_{0.7}Fe_{0.3-x}Nb_xO_{3-\delta}$ perovskite stabilized

by low concentration of Nb for oxygen permeation membrane. *J Membr Sci*. 2008;322:484–490.
22. Zhu X, Wang H, Yang W. Structural stability and oxygen permeability of cerium lightly doped $BaFeO_{3-\delta}$ ceramic membranes. *Solid State Ionics*. 2006;177:2917–2921.
23. Hashim SS, Mohamed AR, Bhatia S. Oxygen separation from air using ceramic-based membrane technology for sustainable fuel production and power generation. *Renew Sust Energ Rev*. 2011;15: 1284–1293.
24. Kharton VV, Shaula AL, Snijkers FMM, Cooymans JFC, Luyten JJ, Yaremchenko AA, Valente AA, Tsipis EV, Frade JR, Marques FMB, Rocha J. Processing, stability and oxygen permeability of Sr(Fe, Al)O_3-based ceramic membranes. *J Membr Sci*. 2005;252: 215–225.
25. Zhu X, Sun S, Cong Y, Yang W. Operation of perovskite membrane under vacuum and elevated pressures for high-purity oxygen production. *J Membr Sci*. 2009;345:47–52.
26. Sunarso J, Baumann S, Serra JM, Meulenberg WA, Liu S, Lin YS, Diniz da Costa JC. Mixed ionic–electronic conducting (MIEC) ceramic-based membranes for oxygen separation. *J Membr Sci*. 2008;320:13–41.
27. Teraoka Y, Zhang H, Furuka S, Yamazoe N. Oxygen permeation through perovskite type oxides. *Chem Lett*. 1985:1743–1746.
28. Shao Z, Yang W, Cong Y, Dong H, Tong J, Xiong G. Investigation of the permeation behavior and stability of a $Ba_{0.5}Sr_{0.5}Co_{0.8}Fe_{0.2}O_{3-\delta}$ oxygen membrane. *J Membr Sci*. 2000;172:177–188.
29. Shao Z, Haile SM. A high-performance cathode for the next generation of solid-oxide fuel cells. *Nature*. 2004;431:170–173.
30. Suntivich J, May KJ, Gasteiger HA, Goodenough JB, Shao-Horn Y. A perovskite oxide optimized for oxygen evolution catalysis from molecular orbital principles. *Science*. 2011;334:1383–1385.
31. Risch M, Stoerzinger KA, Maruyama S, Hong WT, Takeuchi I, Shao-Horn Y. $La_{0.8}Sr_{0.2}MnO_{3-\delta}$ decorated with $Ba_{0.5}Sr_{0.5}Co_{0.8}Fe_{0.2}O_{3-\delta}$: a bifunctional surface for oxygen electrocatalysis with enhanced stability and activity. *J Am Chem Soc*. 2014;136:5229–5232.
32. Arnold M, Gesing TM, Martynczuk J, Feldhoff A. Correlation of the formation and the decomposition process of the BSCF perovskite at intermediate temperatures. *Chem Mater*. 2008;20:5851–5858.
33. Švarcová S, Wiik K, Tolchard J, Bouwmeester HJM, Grande T. Structural instability of cubic perovskite $Ba_xSr_{1-x}Co_{1-y}Fe_yO_{3-\delta}$. *Solid State Ionics*. 2008;178:1787–1791.
34. Müller P, Störmer H, Dieterle L, Niedrig C, Ivers-Tiffée E, Gerthsen D. Decomposition pathway of cubic $Ba_{0.5}Sr_{0.5}Co_{0.8}Fe_{0.2}O_{3-\delta}$ between 700°C and 1000°C analyzed by electron microscopic techniques. *Solid State Ionics* 2012;206:57–66.
35. Mueller DN, De Souza RA, Weirich TE, Roehrens D, Mayer J, Martin M. A kinetic study of the decomposition of the cubic perovskite-type oxide $Ba_xSr_{1-x}Co_{0.8}Fe_{0.2}O_{3-\delta}$ (BSCF) ($x = 0.1$ and 0.5). *Phys Chem Chem Phys*. 2010;12:10320–10328.
36. Li X, Kerstiens T, Torsten M. Oxygen permeability and phase stability of $Ba_{0.5}Sr_{0.5}Co_{0.8}Fe_{0.2}O_{3-\delta}$ perovskite at intermediate temperatures. *J Membr Sci*. 2013;438:83–89.
37. van Veen AC, Rebeilleau M, Farrusseng D, Mirodatos C. Studies on the performance stability of mixed conducting BSCFO membranes in medium temperature oxygen permeation. *Chem Commun*. 2003; 39:32–33.
38. Efimov K, Xu Q, Feldhoff A. Transmission electron microscopy study of $Ba_{0.5}Sr_{0.5}Co_{0.8}Fe_{0.2}O_{3-\delta}$ perovskite decomposition at intermediate temperatures. *Chem Mater*. 2010;22:5866–5875.
39. Müller P, Störmer H, Meffert M, Dieterle L, Niedrig C, Wagner SF, Ivers-Tiffée E, Gerthsen D. Secondary phase formation in $Ba_{0.5}Sr_{0.5}Co_{0.8}Fe_{0.2}O_{3-\delta}$ studied by electron microscopy. *Chem Mater*. 2013;25:564–573.
40. Zhu X, Liu H, Cong Y, Yang W. Permeation model and experimental investigation of mixed conducting membranes. *AIChE J*. 2012;58:1744–1754.
41. Xu SJ, Thomson WJ. Oxygen permeation rates through ion-conducting perovskite membranes. *Chem Eng Sci*. 1999;54:3839–3850.
42. Lin YS, Wang W, Han J. Oxygen permeation through thin mixed conducting solid oxide membranes. *AIChE J*. 1994;40:786–798.
43. Liu Y, Zhu X, Li M, Liu H, Cong Y, Yang W. Stabilization of low-temperature degradation in mixed ionic and electronic conducting perovskite oxygen permeation membranes. *Angew Chem-Int Edit*. 2013;52:3232–3236.

Manuscript received Mar. 16, 2015, and revision received Apr. 20, 2015.